Rab geranylgeranyl transferase α mutation in the *gunmetal* mouse reduces Rab prenylation and platelet synthesis

John C. Detter*, Qing Zhang†, Emilie H. Mules‡, Edward K. Novak†, Vishnu S. Mishra*, Wei Li†, Elzbieta B. McMurtrie*, Velizar T. Tchernev*, Margaret R. Wallace*, Miguel C. Seabra‡, Richard T. Swank†, and Stephen F. Kingsmore*§¶

*Departments of Medicine, Molecular Genetics and Microbiology, Pathology and Laboratory Medicine, and Pediatrics, and Center for Mammalian Genetics, University of Florida, 1600 SW Archer Road, Gainesville, FL 32610; †Department of Molecular and Cellular Biology, Roswell Park Cancer Institute, Carlton and Elm Streets, Buffalo, NY 14263; ‡Division of Biomedical Sciences, Imperial College School of Medicine, Sir Alexander Fleming Building, London SW7 2AZ, United Kingdom; and §Molecular Staging Inc., 66 High Street, Guilford, CT 06437

Edited by John A. Glomset, University of Washington, Seattle, WA, and approved February 11, 2000 (received for review November 29, 1999)

Few molecular events important to platelet biogenesis have been identified. Mice homozygous for the spontaneous, recessive mutation *gunmetal* (*gm*) have prolonged bleeding, thrombocytopenia, and reduced platelet α- and δ-granule contents. Here we show by positional cloning that *gm* results from a G→A substitution mutation in a splice acceptor site within the α-subunit of Rab geranylgeranyl transferase (*Rabggta*), an enzyme that attaches geranylgeranyl groups to Rab proteins. Most Rabggta mRNAs from *gm* tissues skipped exon 1 and lacked a start codon. Rabggta protein and Rab geranylgeranyl transferase (GGTase) activity were reduced 4-fold in *gm* platelets. Geranylgeranylation and membrane association of Rab27, a Rab GGTase substrate, were significantly decreased in *gm* platelets. These findings indicate that geranylgeranylation of Rab GTPases is critical for hemostasis. Rab GGTase inhibition may represent a new treatment for thrombocytosis and clotting disorders.

Platelets play a pivotal role in acute myocardial infarction, unstable angina, deep venous thrombosis, and stroke. About 4 million individuals are hospitalized each year in the United States with these disorders. Treatment with agents that prevent platelet activation reduces the risk of myocardial infarction and stroke by about 30% and death by about 15% (1). Novel platelet antagonists are needed, however, because platelet activation is not always inhibited by current drugs.

Mice homozygous for *gunmetal* (*gm*), a spontaneous, recessive mutation, have prolonged bleeding caused by defects in platelets and megakaryocytes (2, 3). These mice also have macrothrombocytopenia and reduced platelet α- and δ-granule contents (storage pool deficiency, SPD). Megakaryocytes, the progenitors of platelets, are more plentiful in *gm* mice, but have abnormal intracellular membranes, increased emperipolesis, and decreased platelet synthesis. In addition, *gm* homozygotes have partial cutaneous albinism (Fig. 1). These features closely resemble the rare human disorders gray platelet syndrome (GPS) and platelet α,δ-SPD. Positional cloning of *gm* was undertaken both to shed light on the mechanism of disease in platelet SPD disorders and to identify a possible target for antiplatelet drug development.

Materials and Methods

Mice and Genetic Mapping. Mice obtained from The Jackson Laboratory were bred at Roswell Park Cancer Institute. Backcross mice were phenotyped by coat color and genotyped for simple sequence length polymorphisms (SSLPs) and restriction fragment length polymorphism (RFLP) using standard techniques. Linkage relationships were determined by segregation analysis, and best locus order was decided by minimizing crossovers and eliminating double crossovers (4).

Physical Mapping. Mouse yeast artificial chromosome (YAC) and bacterial artificial chromosome (BAC) clones were identified from libraries (Research Genetics, Huntsville, AL) by PCR or hybridization with oligonucleotides corresponding to chromosome 14 loci. Clones were oriented by sequence-tagged site content mapping and insert end-sequencing. Additional markers were isolated by inverse repetitive element PCR (5).

Inverse Repetitive Element-Direct cDNA Selection. Expressed sequences were isolated from YACs by inverse repetitive element-direct cDNA selection (6). Briefly, outward-oriented, biotin-labeled, B1 repetitive element-specific primers were used for long-range PCR of YAC clones (5). Denatured PCR products were incubated with ribosomal DNA, Cot-1 DNA, and yeast DNA, and then with denatured mouse bone marrow cDNA (attached to amplification cassettes). PCR products (and annealed cDNAs) were captured on streptavidin-coated beads and washed stringently, and cDNAs were eluted. Eluted cDNAs were reamplified and used in a second selection cycle. Resultant cDNA fragments were subcloned and sequenced.

Full-Length *Rabggta* (α-Subunit of Rab Geranylgeranyl Transferase) cDNA Isolation. 5′ and 3′ Rapid amplification of cDNA ends (RACE) PCR was performed with mouse fetal brain cDNA (CLONTECH). 5′ RACE used a *Rabggta*-specific reverse primer (5′-TTCACACGCAGACAGCTCTC-3′) and universal forward primer, followed by a second, nested PCR with another *Rabggta* primer (5′-CTCTAGCCTTTTGGCCTCTG-3′) and second universal primer. 3′ RACE was performed by using a *Rabggta*-specific forward primer (5′-CCAGCAGTCTGCTGCACTTC-3′) and universal reverse primer, and a second, nested PCR with the *Rabggta* primer (5′-GGAGCGTTTGGCTGAGATGC-3′) and another universal reverse primer. Products were subcloned and sequenced, and full-length *Rabggta* cDNA sequence was assembled.

This paper was submitted directly (Track II) to the PNAS office.

Abbreviations: *gm*, *gunmetal*; *Rabggta*, α-subunit of Rab geranylgeranyl transferase; GGTase, geranylgeranyl transferase; CHM, choroideremia; GPS, gray platelet syndrome; SPD, storage pool deficiency; YAC, yeast artificial chromosome; BAC, bacterial artificial chromosome; RT-PCR, reverse transcription–PCR; REP, Rab escort protein; [^{3}H]GGPP, [^{3}H]geranylgeranyl pyrophosphate.

Data deposition: The sequences reported in this paper have been deposited in the Mouse Genome Database (accession nos. J:52722 and J:46919) and the GenBank database (accession nos. AF127654, AF127655, AF127656, AF127660, and AF127661).

¶To whom reprint requests should be addressed at: 66 High Street, Guilford, CT 06437. E-mail: stephenk@molecularstaging.com.

The publication costs of this article were defrayed in part by page charge payment. This article must therefore be hereby marked "*advertisement*" in accordance with 18 U.S.C. §1734 solely to indicate this fact.

Article published online before print: *Proc. Natl. Acad. Sci. USA*, 10.1073/pnas.080517697. Article and publication date are at www.pnas.org/cgi/doi/10.1073/pnas.080517697

Fig. 1. C57BL/6J-*gm*/*gm* mice (*Left*) have a lighter coat color than coisogenic C57BL/6J-+/+ mice (*Right*).

Reverse Transcription–PCR (RT-PCR) Analysis. Total RNA was prepared from mouse tissues with equilibrated phenol/guanidine isothiocyanate (GIBCO/BRL). Oligo(dT)-primed, first-strand cDNA was synthesized with SuperScript II (GIBCO/BRL). All *Rabggta* exons were amplified by PCR with gene-specific primers. Aberrant *gm* splicing was identified with *Rabggta* primers 5′-GTGCAAGGGTCCACGGGAC-3′ and 5′-TTCACACG-CAGACAGCTCTC-3′.

Western Blot Analysis. Platelet and bone marrow protein were isolated as described (7) except that platelets were washed twice with 0.38% sodium citrate in 0.85% NaCl and once with 1% ammonium oxalate to remove residual red blood cells. Twenty micrograms of protein in proteinase inhibitor mixture was incubated in SDS/mercaptoethanol and electrophoresed on denaturing 10% polyacrylamide gels, followed by Western blotting on nitrocellulose or poly(vinylidene difluoride) membranes (2). For subcellular fractionation studies, fresh platelets were sonicated and separated into membrane and soluble subcellular fractions by centrifugation as described (2). Samples were immediately separated on 12% polyacrylamide gels. Western blots were probed with specific antisera against Rabggta (8) or Rab27 (9), followed by peroxidase-labeled goat α-rabbit IgG secondary antibody (Kirkegaard & Perry Laboratories), and visualized by incubation with ECL-Plus reagent (Amersham Pharmacia) and autoradiography. Several exposures were taken and comparisons were made in the linear range. Blots were washed and reprobed with antibodies to mouse actin. Alternatively GTP-binding proteins were detected on Western blots by hybridization with [^{32}P]GTP, washing, and autoradiography (2).

Assay of Rab Geranylgeranyl Transferase (GGTase) Activity. Frozen tissues (liver, kidney, or spleen) were thawed, immersed in 3 vol of buffer (50 mM sodium Hepes, pH 7.2/10 mM NaCl/1 mM DTT/0.5 mM PMSF/5 μg/ml aprotinin/5 μg/ml pepstatin/5 μg/ml leupeptin) and lysed by polytron homogenization. Lysates were spun at 100,000 $\times$ *g* for 1 h, and pellets were discarded. Frozen platelet samples (10^7-10^8 platelets) were lysed by repeated passages through a Hamilton syringe. Protein concentrations were determined by using Coomassie Plus reagent (Pierce).

Rab GGTase activity (9) was determined by measuring ^{3}H transfer from [^{3}H]geranylgeranyl pyrophosphate ([^{3}H]GGPP) to Rab1a in 50-μl reactions containing 50 mM sodium Hepes (pH 7.2), 5 mM $MgCl_2$, 1 mM DTT, 4 μM [^{3}H]GGPP, 2,365 dpm/pmol), 5 μM recombinant Rab1a, 2 μM recombinant Rab escort protein (REP) 1, and indicated amounts of cytosolic protein from *gm*/*gm* or +/+ tissues. After incubation for 15 min at 37°C, ethanol/HCl-precipitable radioactivity was measured on glass fiber filters. Assays with concentrations of cytosolic proteins <10 μg were carried out in 25-μl reactions containing 1 μM [^{3}H]GGPP and incubated for 30 min at 37°C.

Assay of GGTase I Activity. GGTase I activity was determined by measuring ^{3}H transfer from [^{3}H]GGPP to Rac1 in a 25-μl reaction containing 50 mM sodium Hepes (pH 7.2), 150 mM KCl, 5 mM $MgCl_2$, 1 mM DTT, 1.2 μM [^{3}H]GGPP, 200 μM Zwittergent 3–14, 25 μM recombinant Rac1, and the indicated amounts of cytosolic proteins (9). After incubation for 30 min at 37°C, ethanol/HCl precipitable radioactivity was measured.

Results and Discussion

Genetic and Physical Mapping of *gm*. Previously, *gm* had been localized to a 1.5-centimorgan (cM) interval on mouse chromosome 14 (10). Genotyping of 29 loci in 2,462 *gm* backcross mice narrowed the *gm* critical region to 0.64 cM between *D14Mit63* and *D14Mit122* (Fig. 2). Three backcrosses were used to minimize the effect of a local recombination cold spot observed in a *Mus spretus* backcross. Genetic markers flanking and within the *gm* critical region were used to isolate contiguous YAC and BAC clones encompassing *gm*. To complete the cloning of the interval, novel, polymorphic simple sequence repeats (*D14Sfk1*, *D14Sfk3*, and *D14Sfk5*) and sequence-tagged sites were isolated from critical region YACs by inverse repetitive element-PCR (5). They were mapped and used to isolate additional YACs and BACs to cover the interval (Fig. 2). A family of serine protease genes (*Mcpt1, Mcpt2, Mcpt4, Mcpt5, Mcpt9, McptL*, *Ctla1, Ctla5, Ctla6, Ctla7*, and *Ctsg*) were mapped to the *gm* critical region but excluded from *gm* candidacy by virtue of incompatible distribution of expression or absence of mutations (data not shown).

Candidate Gene Isolation. Additional candidate genes were identified from pooled *gm* contig YACs and BACs by using a modified direct cDNA selection method (6). Nineteen of 160 selected cDNA fragments were derived from *Rabggta. Rabggta*-derived sequence-tagged sites were physically mapped on six *gm* critical region YAC and BAC clones (Fig. 2). A 2.2-kb *M. spretus* *Bam*HI restriction fragment length polymorphism enabled genetic mapping of *Rabggta* in the *M. spretus* backcross. *Rabggta* cosegregated with *gm* (Fig. 2), confirming derivation from the *gm* critical region.

Because mouse *Rabggta* was novel, cDNAs corresponding to the full-length coding domain were isolated and sequenced. The mouse cDNA shared 94% and 86% nucleotide identity to rat and human *Rabggta*, respectively.

***Rabggta* Mutation Identification.** Analysis of the genomic sequence of *Rabggta* revealed a single difference between C57BL/6J-+/+ and C57BL/6J-*gm*/*gm* DNA: The normal 3′ terminal nucleotide of intron α (guanine) was replaced with an adenine in *gm* DNA (Fig. 3). This substitution created a *Tsp*509I restriction site that was used to show perfect cosegregation of *Rabggta* and *gm* in 2,462 meioses.

***Rabggta* RNA Splicing Defects.** Typically, substitution of the obligatory 3′ terminal guanine of the consensus splice acceptor site prevents normal mRNA splicing and leads to intron retention, exon skipping, or cryptic splice site utilization (11). RT-PCR of the 5′ end of *Rabggta* RNA (corresponding to exons α, 1, and 2) disclosed aberrantly spliced *Rabggta* transcripts in *gm* bone marrow (Fig. 3). This tissue was used because the hematologic abnormalities of *gm* homozygotes are corrected by bone marrow transplantation (3). In normal mice, RT-PCR of the 5′ end of *Rabggta* gave two products. The most abundant product was correctly spliced (exon α - exon 1 - exon 2; Fig. 3, +/+ product a). A second, minor product in normal mice retained intron α (exon α - intron α - exon 1 - exon 2; Fig. 3, +/+ product b) and

GENETICS

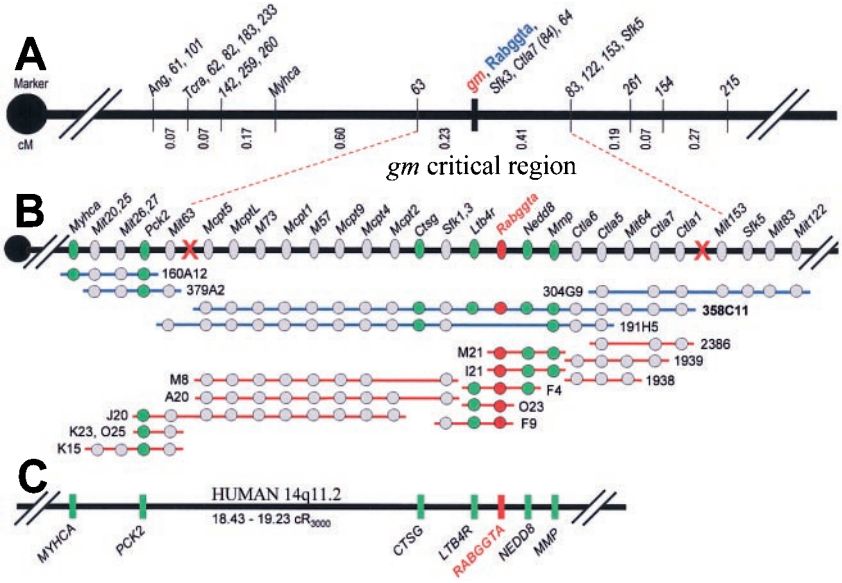

Fig. 2. Genetic and physical maps of mouse chromosome 14 in the vicinity of *gm*. (*A*) Consensus genetic map of the *gm* region on chromosome 14 derived from three backcrosses (MGD J:52722). The circle represents the centromere. Distances between markers are in centimorgans (cM). Numbered loci represent microsatellite markers. Relative positions of loci were ascertained from 769 [(C57BL/6J-*gm* × SPRET)F_1 × C57BL/6J-*gm*], 727 [(C57BL/6J-*gm* × PWK)F_1 × C57BL/6J-*gm*], and 966 [(C57BL/6J-*gm* × DBA)F_1 × C57BL/6J-*gm*] backcross mice. No recombination was found between *gm* and *Rabggta*. Dotted lines link the consensus *gm* genetic map to the physical map. (*B*) Physical map of the *gm* nonrecombinant interval (MGD J:52722). The *gm* critical region is delineated by chromosome crossovers (denoted by red X). *gm* was flanked by *D14Mit63* (proximal), and *D14Mit153* and *D14Mit122* (distal). YAC (blue lines) and BAC (red lines) clones are shown. Loci physically mapped within YAC and BAC clones are indicated with colored circles. The location of *Rabggta* is indicated by red circles. Green circles indicate genes near *gm* that (*C*) also map to the homologous human chromosomal segment (14q11.2).

may be immature, because it could only be marginally detected by RT-PCR with cytosolic or poly(A)$^+$ RNA (data not shown).

In *gm* homozygotes, the major *Rabggta* RT-PCR product of +/+ bone marrow was not observed (product a, exon α - exon 1 - exon 2). Instead, the most abundant *gm* product skipped *Rabggta* exon 1 (Fig. 3, *gm*/*gm* product c; exon α - exon 2). Translation of this transcript was not anticipated to yield functional Rabggta protein because the initiation codon was absent, and no alternative, in-frame start codon was present (Fig. 3).

A second novel, but much less abundant, *gm Rabggta* RT-PCR product represented activation of a cryptic splice donor (within intron α, 84 bp downstream of the normal splice donor site) and acceptor (within exon 1, 13 bp downstream of the G→A substitution) sites (Fig. 3, *gm*/*gm* product d). Utilization of these cryptic splice sites did not result in removal of the initiation codon, and the existence of this transcript may explain the presence of residual Rabggta in *gm* homozygotes.

Like +/+ bone marrow, a rare product that retained intron α occurred in *gm*/*gm* RNA (exon α - intron α - exon 1 - exon 2; Fig. 3, product b′). This *gm*/*gm* transcript also was anticipated to be functional if polyadenylated, because the initiation codon of *Rabggta* is in exon 1, and therefore retention of *gm* intron α (with G→A substitution) should not disrupt translation. However, RT-PCR of cytosolic or poly(A)$^+$ RNA suggested that it was an immature, nonpolyadenylated RNA, like the corresponding transcript in +/+ bone marrow (data not shown).

These aberrant *Rabggta* splice variants were found in all tissues tested (*gm* bone marrow, melanocyte, and kidney; data not shown). As expected, both normal and mutant products were observed in *gm*/+ heterozygote RNA (data not shown). No other defect in splicing was observed in *gm*/*gm*; other regions of *Rabggta* mRNA produced RT-PCR products of expected size and sequence, with the exception of a *Rabggta* isoform that retained intron 9 (in both +/+ and *gm*/*gm* mice).

The enzyme Rab GGTase is composed of Rabggta and a β-subunit (Rabggtb) and absolutely requires Rab escort protein (Rep) 1 or 2 for activity (12, 13). The *gm* reduction in *Rabggta* was specific. Quantitative RT-PCR revealed no changes in the abundance of transcripts of *Rabggtb*, *Rep1* or *Rep2* in *gm*/*gm* bone marrow or kidney (data not shown). Furthermore, Northern blots disclosed no difference between *gm*/*gm* and +/+ tissues in the overall abundance of *Rabggta* mRNA (data not shown).

Rabggta Protein Abundance. Western blots of *gm* platelets showed one consequence of aberrant *Rabggta* mRNA splicing to be ≈70% reduction in 60-kDa Rabggta protein in *gm* platelets compared with +/+ (Fig. 4). It is likely that residual Rabggta protein in *gm*/*gm* platelets resulted from translation of the novel *gm Rabggta* transcript that used cryptic splice sites (Fig. 3, *gm*/*gm* product d).

Rab GGTase Enzymatic Activity. Rab GGTase activity in *gm*/*gm* and +/+ platelets was examined with an *in vitro* assay of Rab1a prenylation (Fig. 4) (9). No other enzyme (including GGTase I and farnesyl-transferase) can prenylate Rab1a (14, 15). *gm*/*gm* Rab GGTase activity was reduced ≈70% compared with +/+ platelets (Fig. 4), matching the decrease in Rabggta protein. Similar results were reproducibly obtained with liver, kidney, and spleen extracts (Fig. 4 and data not shown). The *gm* reduction in Rab GGTase was specific: no difference was observed between *gm*/*gm* and +/+ in activity of GGTase-I, a related but different enzyme (16) (Fig. 4). Thus the *Rabggta* splicing defect in *gm* results in decreased Rabggta and Rab GGTase activity.

Rab27 Hypoprenylation. A previous study showed that gel migration of some small GTP-binding proteins was abnormal in *gm* platelets (2). Novel bands (≈25 and ≈28.5 kDa) of unknown identity were observed on GTP overlays of Western blots of *gm* platelets (Fig. 5) (2). These were not observed in *gm* liver, kidney, brain, spleen, macrophages or neutrophils (2). Rab proteins represented candidates for these abnormal GTP bind-

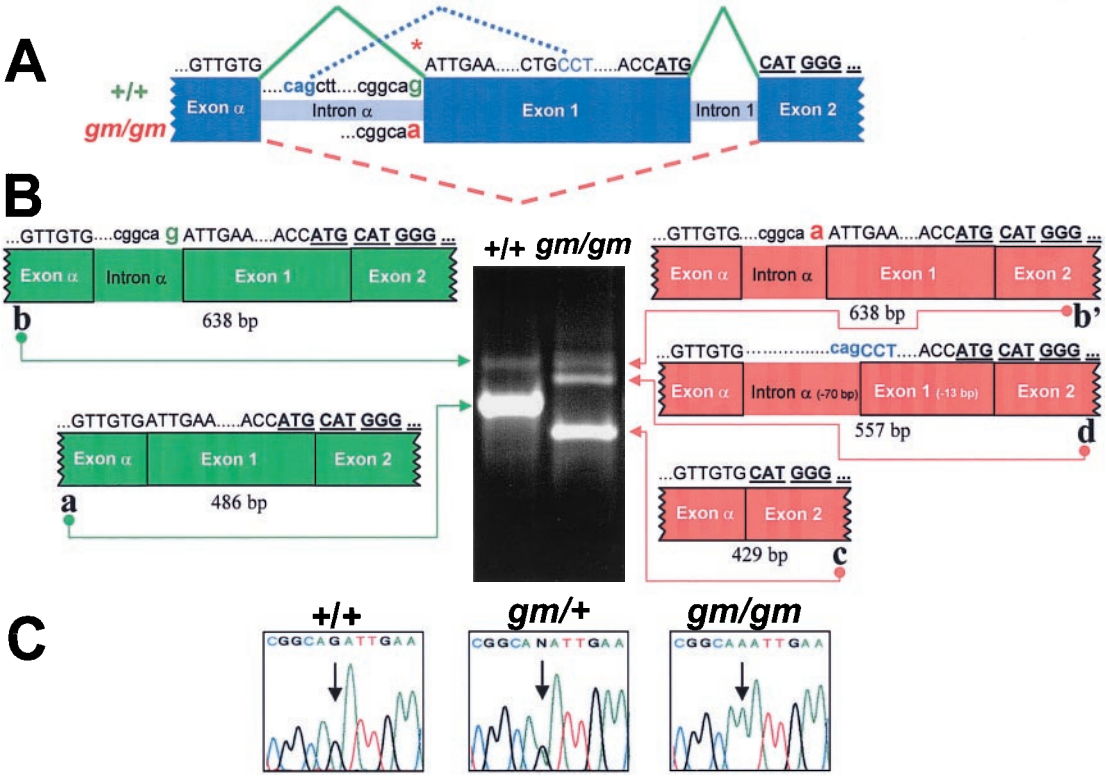

Fig. 3. A splice acceptor mutation in *Rabggta* causes abnormal splicing. (*A*) Genomic structure of the 5′ end of mouse *Rabggta*. Exon α encodes 5′ untranslated region. The initiation methionine (bold and underlined ATG) occurs at the 3′ end of exon 1. *Rabggta* nucleotide sequence above is C57BL/6J-+/+ and below is C57BL/6J-*gm*/*gm*. The splice acceptor mutation is indicated by *. *Rabggta* exons connected by solid green lines represent normal splicing. Dashed red lines indicate exon 1 skipping in *gm*/*gm* RNA, and dotted blue lines indicate cryptic splice sites used by *gm*/*gm*. (B) RT-PCR analysis of RNA from wild-type (+/+) and mutant (*gm*/*gm*) bone marrow. The *Rabggta* oligonucleotides used amplified the region between exon α and exon 2. Each band was excised and sequenced: Normal bone marrow (+/+) shows the expected product of 486 bp (band a) (GenBank accession no. AF127656), and a product (638 bp) retaining intron α (band b) (GenBank accession no. AF127658). *gm*/*gm* bone marrow shows three bands: Band c (429 bp) (GenBank accession no. AF127657) represents exon 1 skipping; band b′ (638 bp) (GenBank accession no. AF127659) retains intron α; band d (557 bp) (GenBank accession no. AF127662) represents utilization of cryptic splice sites in intron α and exon 1. (*C*) Sequence analysis of *Rabggta* genomic DNA. Arrows indicate the splice acceptor mutation: +/+ = G, *gm*/*gm* = A, *gm*/+ exhibits both nucleotides (G and A).

ing proteins. Specifically, Rab27a or Rab27b were excellent candidates because they are abundant in platelets (17). Blots stained with an antibody specific for both Rab27 isoforms disclosed a single band of 27.5 kDa in normal platelets and bone marrow, but an additional, mobility-shifted (28.5 kDa) isoform in *gm*/*gm* (Fig. 5). This isoform may represent unprenylated Rab27 because the electrophoretic mobility of unmodified Rab proteins is slower than prenylated forms in SDS-containing gels (14, 18). Not all small GTPases showed abnormal mobility; no differences between normal and *gm* platelets were observed on immunoblots of Rab4 or Ras (2).

Additional evidence for Rab27 hypoprenylation was sought by examining *gm* platelets for membrane-associated Rab27 (which depends on prenylation) (9). Rab27 was found mainly within the membrane fraction of normal platelets, but predominantly in the soluble fraction of *gm* platelets (Fig. 5). GTP overlay studies showed the distribution and mobility of the abnormal Rab27 band to match that of a previously described "novel" *gm* GTP-binding protein (Fig. 5) (2).

Final evidence for Rab27 hypoprenylation in *gm* platelets was found by immunohistochemisty. Rab27 antibodies labeled punctate structures in normal mouse platelets, consistent with Rab27 localization on intracellular granules (Fig. 5). In contrast, *gm* platelets displayed more diffuse cytoplasmic Rab27 staining (Fig. 5). Collectively, the data suggest that Rab GGTase deficiency in *gm* platelets results in deficient Rab27 prenylation. The existence of other "novel" bands in GTP overlays of Western blots suggests that additional GTP-binding proteins also may be hypoprenylated in *gm* platelets (Fig. 5). Preliminary analyses suggest, as expected, deficiencies in prenylation of other Rabs in *gm* platelets (data not shown).

Correlation of *gm* Genotype and Phenotype. Evidence has been presented that a mutation in *Rabggta*, the *gm* genotype, results in impaired prenylation of Rab GGTase substrates, such as Rab27. Unprenylated Rab proteins lack the ability to attach to membranes and may account for the hematologic phenotype of *gm* (2, 3, 9, 12, 23). Because Rab proteins regulate intracellular protein trafficking and vesicular transport by cycling between membrane-bound and cytosolic forms, failure to attach to intracellular membranes ablates this regulatory activity. Previous studies have documented disordered vesicular transport in *gm* platelets and megakaryocytes: Proteins destined for delivery from the trans-Golgi network to α-granules are misrouted in *gm* platelets (2, 3, 12). As a result, *gm* platelet α-granules lack fibrinogen, von Willebrand factor (vWF) and platelet factor 4. vWF is secreted from *gm* megakaryocytes instead of being transported to α-granules (2). In addition to these qualitative trafficking defects in α- and δ-granules, platelet synthesis is decreased in *gm* mice. Blood platelets are synthesized at the ends of proplatelet processes, long tube-like extensions produced by differentiated megakaryoctyes (24). During platelet assembly the megakaryocyte demarcation membrane system is extensively and dynamically remodeled within the proplatelet processes. Further, platelet production within proplatelet processes critically depends

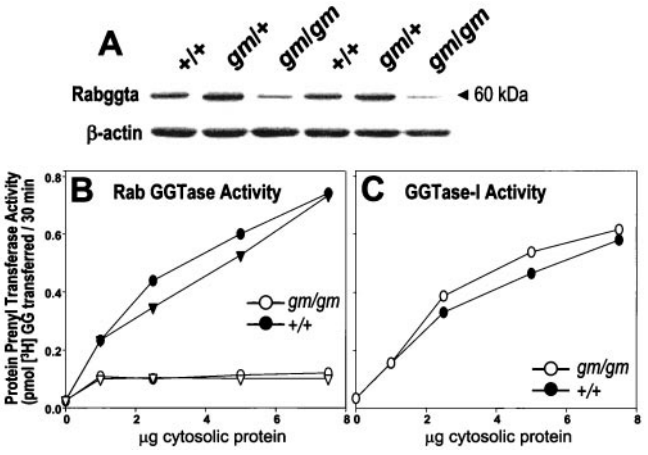

Fig. 4. Decreased Rabggta expression and Rab GGTase activity in *gm*/*gm* mice. (*A*) Western blots of wild-type (+/+), heterozygous (*gm*/+), and mutant (*gm*/*gm*) platelets probed with Rabggta and β-actin antibodies. Rabggta (60 kDa) was reduced ≈70% in *gm*/*gm*. This experiment was repeated four times with the same results. (*B*) Rab GGTase activity of *gm*/*gm* and +/+ platelets. Duplicate cytosolic protein extracts from two samples of pooled platelets from *gm* (open symbols) and C57BL/6J mice (solid symbols) were assayed for Rab GGTase activity by measuring transfer of [^{3}H]geranylgeranyl ([^{3}H]GG) to Rab1a (15). This experiment was repeated four times with platelets, and twice with liver, spleen, and kidney protein extracts with similar results. (*C*) GGTase-I activity of *gm*/*gm* and +/+ pooled platelets. GGTase-I activity was determined by measuring transfer of [^{3}H]GG to Rac1. Each point represents an average of duplicate reactions. For Rab GGTase reactions, a control reaction incubated after addition of 50 mM EDTA was subtracted from all samples. For GGTase-I reactions, a control reaction incubated with buffer alone was subtracted from all samples. These experiments were repeated at least twice in each of the liver, kidney, and spleen extracts with similar results to platelets.

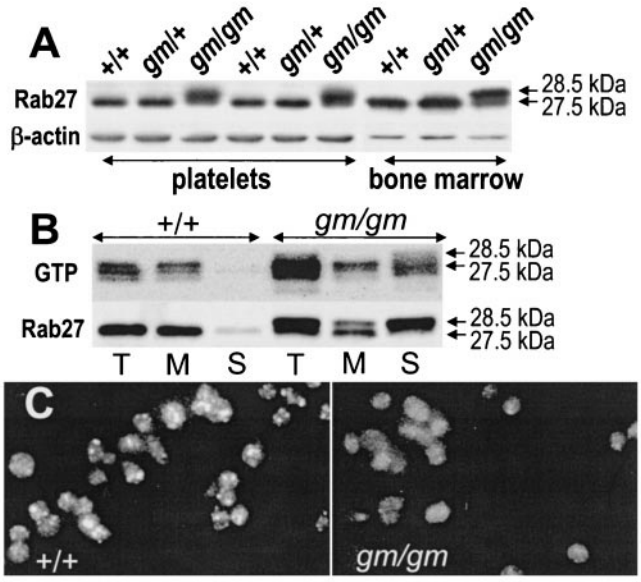

Fig. 5. Deficient prenylation of Rab27 in *gm* platelets. (*A*) Western blots of wild-type (+/+), heterozygous (*gm*/+), and mutant (*gm*/*gm*) platelets and bone marrow incubated with Rab27 and β-actin antibodies. This experiment was repeated five times with the same results. (*B*) Western blots of subcellular fractions of wild-type (+/+) and mutant (*gm*/*gm*) platelets incubated with radiolabeled GTP or Rab27 antibodies. The subcellular fractions were total protein (T), membrane-associated protein (M), and soluble-fraction protein (S). This experiment was repeated five times with similar results. (*C*) Photomicrographs (×200) of +/+ and *gm*/*gm* platelets stained with Rab27 antibodies and detected with a FITC-conjugated secondary antibody. This experiment was repeated three times with similar results.

on both microtubule and actin cytoskeletal components (24). Potential roles of Rab proteins in platelet biogenesis are thus suggested. First, Rab proteins are well known to play key roles in membrane remodeling and trafficking (25). Second, several lines of evidence link Rab-mediated processes of vesicle trafficking with the actin and microtubule-based cytoskeletons (25). Finally, the distribution of membrane complexes is abnormal in *gm* megakaryocytes, and *gm* platelets are larger and more heterogeneous in size than normal (2). Thus, phenotypic effects of *gm* in bone marrow are explicable on the basis of *Rabggta* mutation.

Association of Rab GGTase with maintenance of normal platelet count and bleeding time implies that Rab GGTase represents a novel therapeutic target for thrombocytosis and clotting disorders (such as myocardial infarction, stroke, or deep venous thrombosis). Compounds that selectively inhibit Rab GGTase may be effective in these disorders when administered acutely to mimic *gm* by reducing platelet Rab GGTase activity.

Comparison of *gm* and Choroideremia (CHM). The molecular pathology, but not the phenotype, of *gm* resembles the X-linked human disorder CHM. In both, mutated genes encoding proteins involved in Rab geranylgeranylation result in Rab dysfunction: *Rabggta* is mutated in *gm* and REP1 is mutated in CHM (19, 20). Some Rab GGTase activity is retained in *gm*, probably by aberrant splicing that rescues certain *Rabggta* transcripts. In CHM, partial activity remains because two redundant loci encode REPs (20, 21). In both, a consequence of Rab GGTase deficiency is decreased Rab27 prenylation, as evidenced by change in mobility and membrane association (9). The phenotype of *gm,* however, is different from CHM. Although pigmented tissues are affected in both, *gm* features partial cutaneous albinism whereas CHM has progressive atrophy of the choroid and retina (9). Furthermore, CHM patients do not have prolonged bleeding time or platelet SPD. These differences may reflect genetic complementation by REP2 in CHM, but not *gm*, or species differences as suggested by phenotypic differences between CHM patients and *Chm* knockout mice (22).

Human Platelet SPD Diseases. The human genetic disorders most similar to *gm* are GPS and α/δ-SPD (26). Like *gm*, GPS platelets are reduced in number, are increased in size, and lack α-granule proteins (26–28). Mis-sorting and inappropriate secretion of α-granule proteins occurs in GPS, as in *gm* (28). GPS patients, however, do not exhibit δ-granule storage pool deficiency or partial albinism. Like *gm*, α/δ-SPD is characterized by reduction in the number and contents of both α- and δ-granules (29). *RABGGTA* and *RABGGTB* are excellent candidate genes for GPS and α/δ-SPD.

We thank Lijie Zhen, Shelley Jiang, Diane Poslinski, and Debra Tabaczynski for excellent technical assistance. M.C.S. is a Pew Scholar in the Biomedical Sciences. This work was supported by National Institutes of Health Grants HL51480 and AI39651, E. Matilda Ziegler Foundation for the Blind, and Human Frontier of Science Program.

1. Antiplatelet Trialist's Collaboration (1994) *Br. Med. J.* **308,** 81–106.
2. Swank, R. T., Jiang, S. Y., Reddington, M., Conway, J., Stephenson, D., McGarry, M. P. & Novak, E. K. (1993) *Blood* **81,** 2626–2635.
3. Novak, E. K., Reddington, M., Zhen, L., Stenberg, P. E., Jackson, C. W., McGarry, M. P. & Swank, R. T. (1995) *Blood* **85,** 1781–1789.
4. Green, E. L. (1981) *Genetics and Probabilities in Animal Breeding Experiments* (Macmillan, New York), pp. 77–113.
5. Detter, J. C., Nguyen, Q. A. & Kingsmore, S. F. (1998) *Nucleic Acids Res.* **26,** 4091–4092.
6. Detter, J. C., Mishra, V. S. & Kingsmore, S. F. (2000) *Biotechniques*, in press.

7. Swank, R. T., Reddington, M., Howlett, O. & Novak, E. K. (1991) *Blood* **78,** 2036–2044.
8. Armstrong, S. A., Seabra, M. C., Sudhof, T. C., Goldstein, J. L. & Brown, M. S. (1993) *J. Biol. Chem.* **268,** 12221–12229.
9. Seabra, M. C., Ho, Y. K. & Anant, J. S. (1995) *J. Biol. Chem.* **41,** 24420–24427.
10. O'Brien, E. P., Zhen, L., Jiang, S. Y., Novak, E. K. & Swank, R. T. (1996) *Mamm. Genome* **7,** 206–208.
11. Krawczak, M., Reiss, J. & Cooper, D. N. (1992) *Hum. Genet.* **90,** 41–54.
12. Seabra, M. C. (1998) *Cell Signal* **10,** 167–172.
13. Seabra, M. C., Goldstein, J. L., Sudhof, T. C. & Brown, M. S. (1992) *J. Biol. Chem.* **267,** 14497–14503.
14. Kinsella, B. T. & Maltese, W. A. (1991) *J. Biol. Chem.* **266,** 8540–8544.
15. Wilson, A. L, Erdman, R. A, Castellano, F. & Maltese, W. A. (1998) *Biochem. J.* **333,** 497–504.
16. Casey, P. J. & Seabra, M. C. (1996) *J. Biol. Chem.* **271,** 5289–5292.
17. Chen, D., Guo, J., Miki, T., Tachibana, M. & Gahl, W. (1997) *Biochem. Mol. Med.* **60,** 27–37.
18. Sanford, J. C., Foster, L., Kapadia, Z. & Wessling-Resnick, M. (1995) *Anal. Biochem.* **224,** 547–556.
19. Seabra, M. C., Brown, M. S., Slaughter, C. A., Sudhof, T. C. & Goldstein, J. L. (1992) *Cell* **70,** 1049–1057.
20. Seabra, M. C., Brown, M. S. & Goldstein, J. L. (1993) *Science* **259,** 377–381.
21. Cremers, F. P., Armstrong, S. A., Seabra, M. C., Brown, M. S. & Goldstein, J. L. (1994) *J. Biol. Chem.* **269,** 2111–2117.
22. van den Hurk, J. A., Hendriks, W., van de Pol, D. J., Oerlemans, F., Jaissle, G., Ruther, K., Kohler, K., Hartmann, J., Zrenner, E., van Bokhoven, H., *et al.* (1997) *Hum. Mol. Genet.* **6,** 851–858.
23. Novick, P. & Zerial, M. (1997) *Curr. Opin. Cell Biol.* **9,** 496–504.
24. Italiano, J. E., Jr., Lecine, P., Shivdasani, R. A. & Hartwig, J. H. (1999) *J. Cell Biol.* **147,** 1299–1312.
25. Schimmoller, F., Simon, I. & Pfeffer, S. R. (1998) *J. Biol. Chem.* **273,** 22161–22164.
26. Swank, R. T., Novak, E. K., McGarry, M. P., Rusiniak, M. E. & Feng, L. (1998) *Pigment Cell Res.* **11,** 60–80.
27. Cramer, E. M., Vainchenker, W., Vinci, G., Guichard, J. & Breton-Gorius, J. (1985) *Blood* **66,** 1309–1316.
28. Smith, M. P., Cramer, E. M. & Savidge, G. F. (1997) *Baillieres Clin. Haematol.* **10,** 125–148.
29. Weiss, H. J., Witte, L. D., Kaplan, K. L., Lages, B. A., Chernoff, A., Nossel, H. L., Goodman, D. S. & Baumgartner, H. R. (1979) *Blood* **54,** 1296–1319.